Desalination and Water Treatment
www.deswater.com

doi: 10.5004/dwt.2017.1579

58 (2017) 298–307
January

Photo-degradation and photo-mineralization of reactive brilliant orange KN-5R by nano-photocatalyst–modified 3D fabrics

Seyed Majid Ghoreishian[a,*], Mohammad Norouzi[b], Khashayar Badii[c]

[a]*Young Researchers and Elite Club, South Tehran Branch, Islamic Azad University, Tehran, Iran, Tel. +98 21 88347425; email: m.ghoreishian.1985@gmail.com*

[b]*Graduate Program of Biomedical Engineering, University of Manitoba, Winnipeg, MB, Canada, Tel. +1-204-295-3410; email: norouzim@myumanitoba.ca*

[c]*Institute of Colorants, Paints and Coatings (ICPC), Tehran, Iran, Tel. +98 2122969777; email: badii@icrc.ac.ir*

Received 27 October 2015; Accepted 14 June 2016

ABSTRACT

In this study, ZnO, TiO_2 and ZnO/TiO_2 nano-photocatalysts (nphs) were loaded into 3-dimensional fabrics (spacer fabrics) for photo-decolorization and photo-mineralization of Reactive Brilliant Orange KN-5R (RBO KN-5R). Surface morphology and the presence of nphs on the spacer fabrics were studied utilizing SEM and FTIR, respectively. Also, the effect of main operational parameters on the decolorization efficiency was investigated and the process was optimized. Furthermore, total organic carbon (TOC) analysis was employed to scrutinize the photo-mineralization of the dye. Complete decolorization, high efficient mineralization and 90% TOC reduction were achieved in the case of ZnO/TiO_2 nphs after 120 min of UV light irradiation. Also, the kinetic analyses indicated that the photocatalytic decolorization rate followed the Langmuir–Hinshelwood kinetic model. The results revealed that the spacer fabrics loaded with ZnO/TiO_2 nphs can be considered as an effective system for decolorization and TOC reduction of reactive dyes in textile wastewater.

Keywords: Textile wastewater; Photo-decolorization; Photo-mineralization; 3-dimensional textile; Reactive dye

1. Introduction

Most of the modern dyes consist of toxic compounds. Therefore, colored wastewater produced by textile industry is categorized as one of the major sources of environmental contamination and a serious hazard to aquatic living organisms [1,2].

Among the broad range of dyes which are used in textile industry, reactive dyes have been favored owing to their desirable fastnesses and brilliant hues [3]. Reactive dyes, as a result of their conjugated aromatic compounds and complicated chemical structure, are resistant to destruction by conventional treatment methods. Therefore, it is urgent to develop various effective and innovative technologies in order to complete degradation of reactive dyes [4,5].

Advanced oxidation processes (AOPs) have been known as a promising approach because of their effectiveness, operational simplicity, as well as, low temperature and low energy requirements. These processes are composed of several techniques such as Fenton, photo-Fenton, Fenton-like and photocatalytic processes [6].

Meanwhile, AOPs using heterogeneous catalysis have attracted more attention. This technique is fundamentally based on the irradiation of ultraviolet (UV) light on nano-photocatalysts (nphs) to generate reactive species such as hydroxyl radicals ($OH^{\bullet}$), which oxidizes a broad range of organic pollutants quickly and non-selectively [7–10]. In fact, UV irradiation generates electron-hole $\left(e^{-}_{CB}/h^{+}_{VB}\right)$ pairs in the conduction band (CB) and the valence band (VB) of nphs, respectively (Eq. (1)). The excited electron reacts with the oxygen adsorbed on the surface of the nphs which leads to the formation of superoxide radical anion ($O_2^{\bullet -}$) (Eq. (2)) [11].

* Corresponding author.

The hole in the VB can also react directly with contaminant or generate OH• (Eqs. (3) and (4)) [12].

$$SMO_{(s)} + h\upsilon \xrightarrow{\lambda < 390\ nm} SMO\,(e^-_{CB} + h^+_{VB}) \quad (1)$$

$$e^-_{CB} + O_2 \rightarrow O_2^{\bullet -} \quad (2)$$

$$h^+_{VB} + \text{dye} \rightarrow \text{dye}^{\bullet +} \rightarrow \text{oxidation of the dye} \quad (3)$$

$$h^+_{VB} + H_2O \rightarrow H^+ + OH^\bullet \quad (4)$$

Nowadays, TiO_2 nanoparticles (NPs) have found wide applications in eliminating gaseous and aqueous contaminants because of their good photocatalytic properties, cost-effectiveness and stability [13,14]. In addition, because of the quantum efficiency and the ability to produce H_2O_2 more efficiently than other nphs, ZnO NPs can be considered as an alternative to TiO_2 NPs in the photocatalytic processes [2,15].

Elimination of environmental contamination by nphs comprises two typical approaches including suspension of nphs in solutions and loading of nphs on surfaces [2]. Amid those, the loading of nphs on surfaces is preferred, because it excises the catalyst separation and recycling from the treated wastewater after the detoxification, which makes it suitable for industrial applications [16].

Various kinds of surfaces such as ceramic, carbon, glass, metal and bio-absorbent have been employed as a substrate in order to load nphs for photocatalytic processes [17–19]. Recently, Ghoreishian et al. [3,8] reported the loading of nphs on 3-dimensional fabrics (spacer fabrics) for the photocatalytic removal of dyes.

Spacer fabric is defined as fabrics which have two external surfaces connected to each other with spacer yarns. Because of the 3-dimensional structure of the spacer fabric, mass transfer occurs in the middle parts in addition to the surfaces. Furthermore, due to the existence of the yarns connecting the up and down two layers of the spacer fabric, passing of wastewater in these parts is slower than the surfaces which leads to providing more time for the photocatalytic process. Moreover, due to the lack of affinity between reactive dyes and polyester fabric, their interaction in the photocatalytic processes is negligible [20–26].

The aim of this study was to evaluate the heterogeneous photo-decolorization and photo-mineralization of Brilliant Orange KN-5R (RBO KN-5R) using loaded ZnO, TiO_2 and ZnO/TiO_2 nphs on the porous structure of spacer fabric. The effects of operational parameters on the efficiency of the decolorization were investigated. Furthermore, the kinetics of the photo-decolorization was studied.

2. Materials and methods

2.1. Chemicals

The spacer fabric (a surface string of 150 den, a beneath string of 150 den, a mono-filament connector string of 30 den, a weight of 255 g/m^2 and a thickness of 9 mm) was supplied from Bonyad Fiber Production Co., Iran (Fig. 1). Nano-powder of ZnO (average size of < 50 nm, zincite) and nano-powder of TiO_2 (Degussa P-25) (average size of 21 nm, purity of 97%, 80% anatase and 20% rutile) were provided from Sigma-Aldrich, USA, and Evonik, Germany, respectively. RBO KN-5R (molecular weight: 617.53 g/mol), an anionic mono-azo dye, was purchased from Alvan Sabet Co., Iran, and the chemical structure is shown in Fig. 2. The λ_{max} of RBO KN-5R was 494 nm. Citric acid mono-hydrate (CA, $C_6H_8O_7.H_2O$) as a cross-linking agent, hydrogen peroxide (30%), sodium chloride, sodium sulfate, sodium bicarbonate, PEG400 (polyethylene glycol 400) as an anticoagulant agent, hydrochloric acid (37%) and sodium hydroxide were all purchased from Merck, Germany. Sodium hypophosphite (SHP, $NaH_2PO_2.H_2O$) as a catalyst was supplied from Sigma-Aldrich, USA. All of the chemicals were of analytical grade.

2.2. Apparatus

The decolorization efficiency was determined by measuring the absorbance of the dye at the λ_{max} at different time intervals by UV–vis spectrophotometer (Lambda 25, Perkin-Elmer, USA). Scanning electron microscopy (SEM, LEO 1455VP, Cambridge, UK) was used for morphology observation. All the specimens were sputter-coated with gold prior to SEM observation. Fourier transform infrared (FTIR) spectra were observed in the range of 400–4,000 cm^{-1} using a Nicolet IR100 FT-IR (Madison, WI, USA). Total organic carbon (TOC) was determined by a total organic carbon analyzer (TOC-VCPH, Shimadzu, Japan). A pH meter (Hach Co., USA) was employed to determine the initial pH of the solutions. Fritsch ultrasonic bath (Laborette 17, Fritsch GmbH, Germany) was also used to a produce homogenous solution of the nphs and the chemicals. An air-circulating oven (Memmert, Germany) was used to cure the chemicals on the samples.

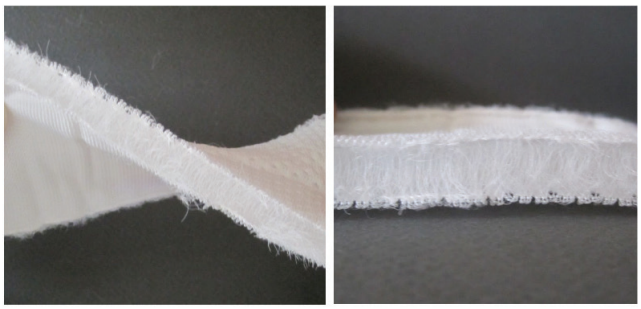

Fig. 1. Photograph of spacer.

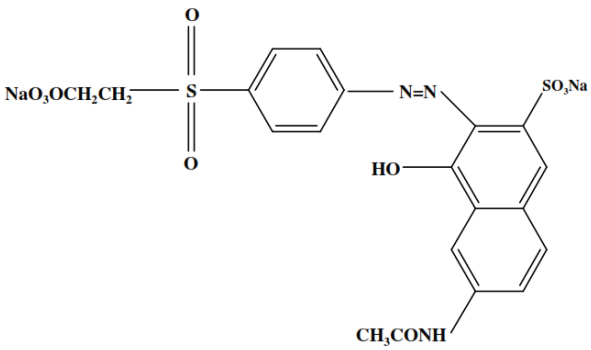

Fig. 2. Chemical structure of RBO KN-5R.

Table 1
Preparation of various spacer samples

Sample	Nphs ratio	SHP (mg/L)	CA (mg/L)
1	ZnO	0.6	1
2	[ZnO/TiO_2] = 1:1	0.6	1
3	TiO_2	0.6	1

2.3. Procedure

Nphs can be loaded on the surface of the textiles by carboxylic acids such as succinic acid (SA), maleic acid (MA), 1,2,3,4-butane tetracarboxylic acid (BTCA) and citric acid (CA) as stabilizer according to the methods reported by the others [27,28]. Padding technique as a simple method was used for treatment of the textile with the NPs. In this method, aqueous solutions containing 50wt% of the nphs with respect to the textile weight, 10wt% CA, 6wt% SHP and PEG 400 were prepared in L:G (Liquid to Good Ratio)≡40:1. The nphs, SHP and CA content have been presented in Table 1. The prepared solutions containing nphs and the other chemicals were sonicated for 15 min to obtain the well-dispersed solutions. Then, the spacer fabrics were impregnated in the prepared solutions and sonication process was continued for 15 min. Thereafter, the treated samples were passed through a pad mangle (with 90% wet pick-up). Finally, the treated samples were dried at 100°C for 8 min followed by curing at 140°C for 4 min.

2.4. Photo-decolorization procedure

Photo-decolorization processes were conducted in a photoreactor under UV irradiation (peak wavelength of 254 nm) at 25 ± 1°C as described in our previous work [3]. The degree of degradation of RBO KN-5R was calculated by Eq. (5):

$$\text{Degradation (\%)} = \frac{C_0 - C_t}{C_0} \times 100 \quad (5)$$

where C_0 is the initial dye concentration (mg/L) and C_t is the concentration of dye at time t (mg/L).

3. Results and discussion

3.1. SEM images

Morphology of the samples was observed by SEM. Fig. 3 (a)–(f) illustrates the SEM images of nano-ZnO powder (3a), nano-TiO_2 powder (3b), untreated spacer fabric (3c), treated spacer fabric with ZnO/SHP/CA (3d), ZnO/TiO_2/SHP/CA (3e) and TiO_2/SHP/CA (3f). Generally, the images confirmed the presence of nphs on the surface of the treated spacer fabrics. It can be seen that ZnO and TiO_2 nphs widely covered the surface of the samples confirming homogeneous deposition of the nphs on the surface of the spacer fabrics. However, the agglomeration of nphs may be attributed to the thermo-migration of the nphs during the curing process. Moreover, the results clearly showed that surface morphology of the spacer fabrics changed after the treatment.

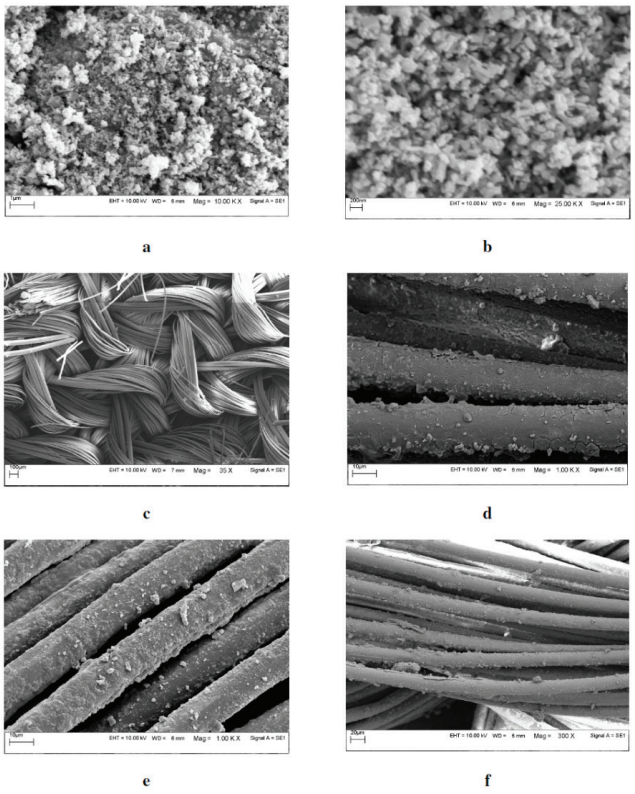

Fig. 3. SEM images of the (a) nano-ZnO powder, (b) nano-TiO_2 powder, (c) untreated spacer fabric, treated spacer fabric with (d) ZnO/SHP/CA, (e) ZnO/TiO_2/SHP/CA and (f) TiO_2/SHP/CA.

3.2. FTIR analysis

To verify the functionalization of the spacer fabric by the nphs, the untreated and treated spacer fabrics were studied with the FTIR technique (Fig. 4). The untreated sample (Fig. 4(a)) showed the main absorption bands at 722 cm^{-1} (ring C–H out-of-plane bending), 857 cm^{-1} (ring C–C out of plane bending vibrations), 1,017 cm^{-1} (O-H out of plane bending in terminal carboxylic groups in polyester chains), 1,091 cm^{-1} (glycol C–O stretching), 1,244 cm^{-1} (C=O in-plane bending) and 1,709 cm^{-1} (stretching vibration band of ester carbonyl (C=O) group) [29]. After the treatment with SHP and CA, new peaks could be observed at 955 cm^{-1} and 1,338 cm^{-1} corresponding to –OH plane deformation vibration and carboxylate stretching in CA, respectively [30]. All the strengthened absorption peaks indicate that some polar groups were added to the spacer (Fig. 4(b)). The treated spacers with ZnO/SHP/CA, ZnO/TiO_2/SHP/CA and TiO_2/SHP/CA (Figs. 4(c)–(e)) showed distinctive peaks at 535 cm^{-1} and 669 cm^{-1} corresponding to ZnO and TiO_2 stretching, respectively [31,32]. This reveals that the nphs were loaded on the spacer fabric surface as it was expected.

3.3. Effect of pH

In general, the efficiency of photocatalytic treatment depends upon the pH of the reaction solution. The photo-decolorization efficiency of ZnO/TiO_2 system was determined in the pH range of 2.0–10.0 (Fig. 5). As shown in Fig. 5,

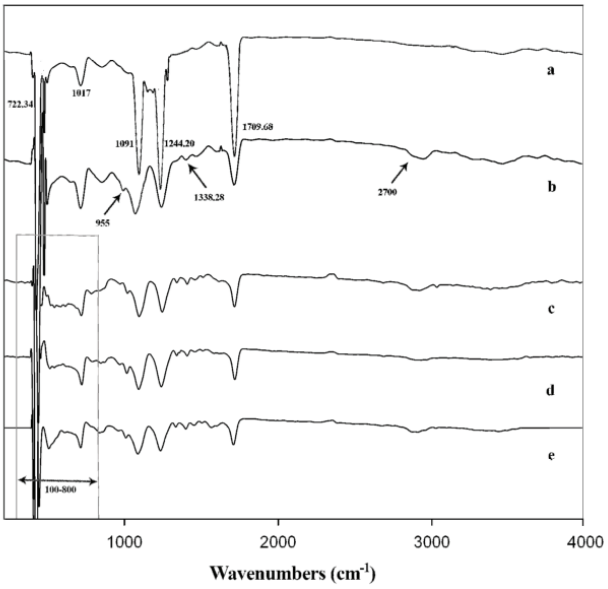

Fig. 4. FTIR spectra of (a) untreated spacer, treated spacer with (b) SHP/CA, (c) ZnO/SHP/CA, (d) ZnO/TiO_2/SHP/CA and (e) TiO_2/SHP/CA.

the dye removal efficiency followed the order of pH_{acidic} > $pH_{natural}$ > $pH_{alkaline}$.

Although several mechanisms have been suggested for explaining the effect of pH on the efficiency of photo-decolorization of the dyes, the effect of pH of zero point charge (pH_{zpc}) and its relation to the ionic form of the organic dye (anionic or cationic) have been preferred. At pH_{zpc}, surface of the nphs is uncharged (pH_{zpc} 9 for ZnO and pH_{zpc} 6.7 for TiO_2); hence, the surface of the catalyst is positively and negatively charged at lower pH_{zpc} and higher pH_{zpc}, respectively [33,34]. RBO KN-5R molecule possesses sulfonic and [2-(sulfoxy) ethyl] sulfonyl groups as the reactive groups, both of which are negatively charged in the solution. Therefore, it results in an electrostatic interaction between the catalyst surface and the dye molecules in lower values of zpc, leading to initiation of the photo-decolorization process [11,35].

On the other hand, at lower pH values, photo-corrosion of ZnO takes place which would result in reducing the efficiency of dye decolorization. At pH < 6, soluble ZnO includes Zn^{2+} and $Zn(OH)^+$. The formation of Zn^{2+} is attributed to the oxidation of ZnO by h^+_{VB} (Eqs. (6)–(8)) [36,37]. In fact, at lower pH, surface ions and small clusters can easily escape from the lattice structure.

$$ZnO_{(s)} + 2H^+_{(aq)} \leftrightarrow Zn^{2+}_{(aq)} + H_2O_{(l)} \quad (6)$$

$$ZnO_{(s)} + H^+_{(aq)} \leftrightarrow Zn(OH)^+_{(aq)} \quad (7)$$

$$ZnO + 2h^+_{VB} \rightarrow Zn^{2+} + O \quad (8)$$

It can be concluded from Fig. 5 and Eqs. (6)–(8) that pH 2 was the most effective in decolorization. However, as reaching pH 2 is not cost-effective on an industrial scale and due to the fact that the photo-corrosion of ZnO occurs at pH levels

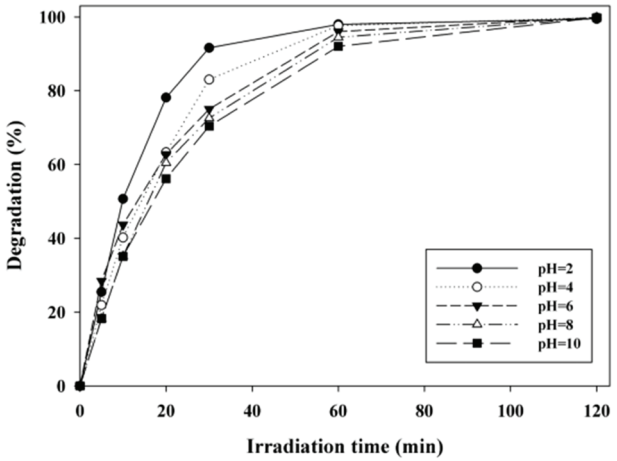

Fig. 5. Effect of pH on the photo-decolorization of RBO KN-5R: $[RBO\ KN\text{-}5R]_0$ = 40 mg/L, $[H_2O_2]_0$ = 100 mg/L, ZnO/TiO_2.

lower than 4, pH 6 was chosen as the optimum value for the decolorization experiments.

3.4. Effect of initial H_2O_2 concentration

Several studies have been done on the usage of hydrogen peroxide as an electron acceptor that suppress the recombination of photo-generated $\left(e^-_{CB}/h^+_{VB}\right)$ pair in nphs efficiently by increase the formation of $OH^\bullet$ (Eqs. (9)–(12)) [12,38,39].

$$H_2O_2 + h\upsilon \rightarrow 2OH^\bullet \quad (9)$$

$$H_2O_2 + 2h^+_{VB} \rightarrow O_2 + 2H^+ \quad (10)$$

$$H_2O_2 + e^- \rightarrow OH^- + OH^\bullet \quad (11)$$

$$H_2O_2 + O_2^- \rightarrow OH^- + OH^\bullet + O_2 \quad (12)$$

Determination of optimum concentration of H_2O_2 is an important parameter from technical and industrial points of view. Excess amount of H_2O_2 can also become a scavenger of $OH^\bullet$ (Eqs. (13)–(15)) [12,40,41].

$$H_2O_2 + 2OH^\bullet \rightarrow 2H_2O + O_2 \quad (13)$$

$$H_2O_2 + OH^\bullet \rightarrow H_2O + HO_2^\bullet \quad (14)$$

$$HO_2^\bullet + OH^\bullet \rightarrow H_2O + O_2 \quad (15)$$

As shown in Fig. 6, with the increase in H_2O_2 concentration from 50 to 100 mg/L, the efficiency of the dye decolorization increased. However, there was no difference between the decolorization resulted from the initial concentration of 100 and 150 mg/L of H_2O_2. Therefore, 100 mg/L was chosen as the optimum concentration of H_2O_2 for the maximum decolorization of RBO KN-5R.

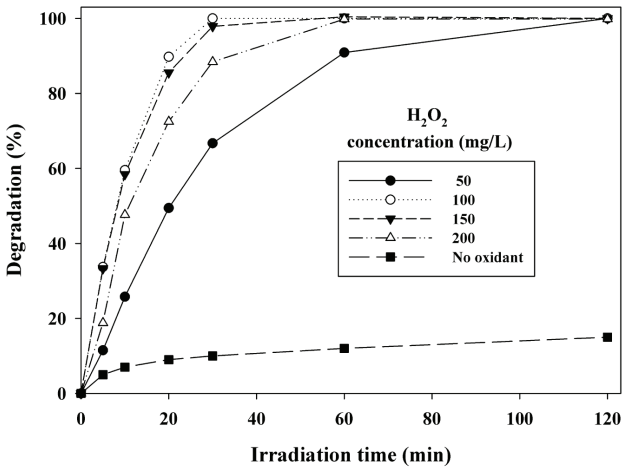

Fig. 6. Effect of the initial concentration of H_2O_2 on the photo-decolorization efficiency: pH 6, $[RBO\ KN\text{-}5R]_0$ = 40 mg/L, ZnO/TiO_2.

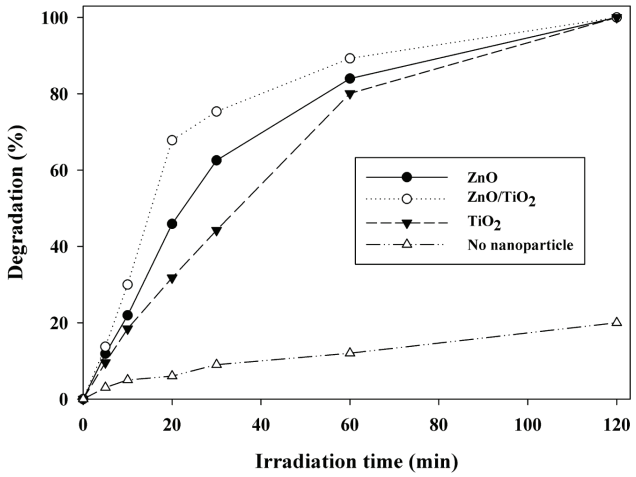

Fig. 7. Effect of the nphs composition on the photo-decolorization: pH 6, $[RBO\ KN\text{-}5R]_0$ = 40 mg/L, $[H_2O_2]_0$ = 100 mg/L.

3.5. Effect of nphs

According to Table 1, various compositions of the nphs were employed. Fig. 7 shows the efficiency of the dye photo-decolorization after 120 min at pH 6, dye initial concentration of 40 mg/L and initial H_2O_2 concentration of 100 mg/L. The decolorization efficiency of the sample treated with ZnO/TiO_2 after 30 min was almost 80%, while for ZnO and TiO_2, it was 60% and 40%, respectively. It can be concluded that, the spacer fabric treated with ZnO/TiO_2 showed superior performance in the elimination of the dye under UV illumination. Due to the similarity in energy gap of ZnO and TiO_2, they demonstrated a synergistic effect in their mixture [42,43]. Fig. 7 shows that the samples treated with ZnO showed higher efficiency in comparison with the ones treated with TiO_2. This can be related to the ability of ZnO nphs in more absorption of UV light in comparison with TiO_2, especially at the wavelength lower than 385 nm [44].

3.6. Effect of initial dye concentration

To evaluate the effect of the dye concentration on efficiency of the degradation process, the dye concentration was varied in a range of 40 to 80 mg/L for each of the samples and the results were shown in Fig. 8.

It was observed that the photocatalytic removal of RBO KN-5R decreased with an increase in the initial dye concentration. The reasons of the reverse relation between the dye removal efficiency and the dye initial concentration can be explained on the following basis [45,46]:

(1) At high concentration of the dye, due to the engagement of active sites of the nphs by the dye molecules, the formation of $OH^{\bullet}$ decreases which results in a decreased efficiency of the process.
(2) With an increase in dye concentration, the molecules of the dye act as blocking agents for UV radiation. Therefore, lower UV rays penetrate the solution, leading to the less excitation of the nphs and decrease in electron-hole formation. In addition, the formation of $OH^{\bullet}$ and superoxide radical anion $(O_2^{\bullet -})$ decreases.

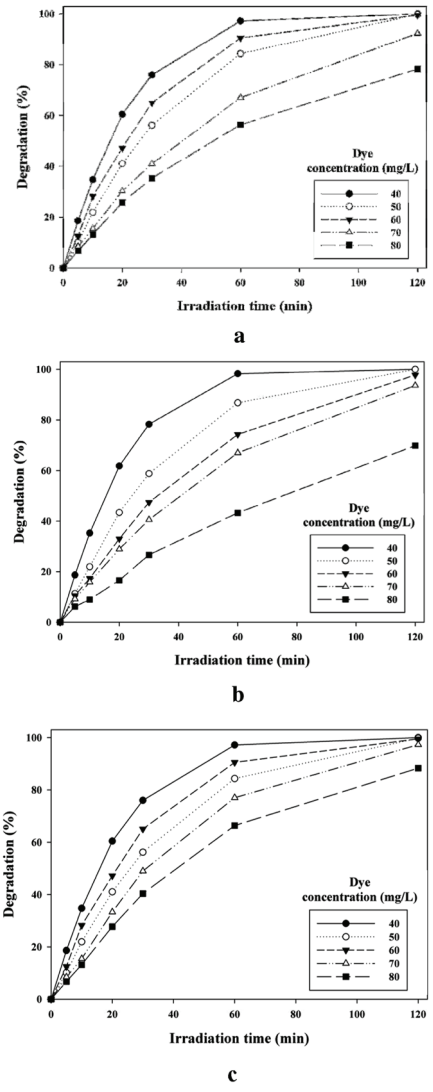

Fig. 8. Effect of the initial dye concentration on the photo-decolorization: (a) ZnO (b) ZnO/TiO_2 (c) TiO_2.

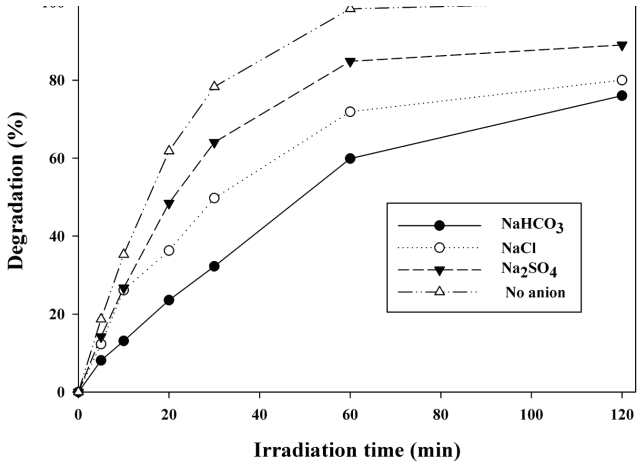

Fig. 9. Effect of anion (NaCl, Na_2SO_4 and $NaHCO_3$) on the photo-decolorization: pH 6, $[RBO\ KN\text{-}5R]_0$ = 40 mg/L, [anion] = 10 mg/L, $[H_2O_2]_0$ = 100 mg/L, ZnO/TiO_2.

(3) With an increase in the dye concentration, the intermediate products formed by the dye degradation in the solution increase. These products and molecules of the dye in the solution compete with H_2O_2 to occupy the active sites, which results in a decreased photo-decolorization efficiency.

3.7. Effect of anions

As the auxiliary chemicals such as salts have extensive applications in textile dyeing and printing, their presence in dye-containing wastewater is common. These substances may compete with molecules of the dye for the active sites on the nphs surface and subsequently, decrease the degradation rate of the target dyes. Additionally, they may act as light screens, thus reducing the photon receiving efficiency to the surface of nphs. Moreover, anions compete with molecules of the dye to react with oxidative radicals. Therefore, the required amount of H_2O_2 increases to provide sufficient $OH^\bullet$ in order to completely support the degradation reactions [41,45]. To evaluate the effect of anions, NaCl, Na_2SO_4 and $NaHCO_3$ (10 mg/L) were used. As it can be seen in Fig. 9, the effectiveness of the photo-degradation system decreased in the presence of the inorganic anions. The observed detrimental effect on the photo-degradation of RBO KN-5R obeyed the following order: $SO_4^{2-} < Cl^- < HCO_3^-$. The mechanisms of their performance were summarized in Eqs. (16)–(22) [41,47,48].

$$Cl^- + OH^\bullet \rightarrow Cl^\bullet + OH^- \quad (16)$$

$$Cl^\bullet + Cl^- \rightarrow Cl_2^{\bullet-} \quad (17)$$

$$Cl_2^{\bullet-} + dye \rightarrow dye^{\bullet+}(intermediate) + 2Cl^- \quad (18)$$

$$SO_4^{2+} + h_{VB}^+ \rightarrow SO_4^{\bullet-} \quad (19)$$

$$SO_4^{\bullet-} + dye \rightarrow SO_4^{2-} + dye^{\bullet+}(intermediate) \quad (20)$$

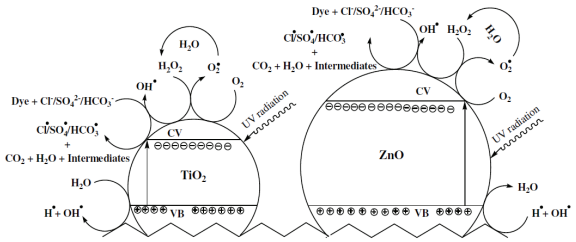

Fig. 10. Schematic interaction of RBO KN-5R, anions and nphs.

$$HCO_3^- + OH^\bullet \rightarrow CO_3^{\bullet-} + H_2O \quad (21)$$

$$CO_3^{\bullet-} + OH^- \rightarrow CO_3^{2-} + OH^\bullet \quad (22)$$

Although the radicals produced by the anions are capable of oxidizing RBO KN-5R, they are not as active as $OH^\bullet$ and h_{VB}^+ [49,50].

The $SO_4^{\bullet-}$, Cl^∞ and $HCO_3^{\bullet-}$ radicals generated in Eqs. (16), (19) and (22) have a lower redox potential than hydroxyl radicals ($E_0(SO_4^{\bullet-}/SO_4^{2-}) = 2.6$ V, $E_0(Cl^\bullet/Cl^-) = 2.47$ V, $E_0(CO_3^{\bullet-}/CO_3^{2-}) = 1.85$ V and $E_0(^\infty OH / H_2O) = 2.80$ V). Therefore, the degradation rate of RBO KN-5R considerably reduced by the presence of inorganic ions. On the other hand, the opposing effects of chloride and sulfate were mainly due to the adsorption whereas in the case of bicarbonate, the parallel effects of light attenuation, competition for active sites (surface deactivation) and their tendency to act as scavengers of $OH^\bullet$ resulted in a prolonged photo-decolorization [34,45]. Furthermore, the negative effect of bicarbonate anion can be attributed to the shift of pH from weak acidic to weak alkaline inhibiting complete photo-decolorization [51]. The effects of the dye and the anions on the photocatalytic decolorization of RBO KN-5R have been shown in Fig. 10.

3.8. Kinetic analysis of dye decolorization

Several studies indicated that the photo-degradation of various reactive dyes with semiconductors fitted the Langmuir–Hinshelwood kinetic model (Eq. (23)) [52]:

$$r = -\frac{dC_t}{dt} = \frac{K_{ads}k_{L-H}C_t}{1+K_{ads}C_t} \quad (23)$$

where r is the rate of dye decolorization (mg/L min), C_t the concentration of the dye (mg/L) at time t, t is the time of irradiation (min), k_{L-H} is the reaction rate constant and K_{ads} is the dynamic Langmuir adsorption constant [53]. The integrated form of the Eq. (23) can be mentioned as follows for $C = C_0$ at $t = 0$ (Eq. (24)) [54]:

$$t = \frac{1}{K_{ads}k_{L-H}}\ln\left(\frac{C_0}{C_t}\right) + \frac{1}{k_{L-H}}(C_0 - C_t) \quad (24)$$

where C_0 is the initial concentration of the dye and C_t is the dye concentration in the solution after treatment (mg/L). Because the dye concentration is very low, Eqs. (25) and (26) were obtained [51,54].

$$t = \frac{1}{K_{ads}k_{L\text{-}H}}\ln\left(\frac{C_0}{C_t}\right) \quad (25)$$

$$\ln\left(\frac{C_0}{C_t}\right)=K_{ads}k_{L\text{-}H}t \quad (26)$$

By supposing $k_{app}= K_{ads}\ k_{L\text{-}H}$, the first-order kinetic equation (Eq. (27)) was obtained where k_{app} represents the apparent first order rate constant [7].

$$\ln\left(\frac{C_0}{C_t}\right)=k_{app}t \quad (27)$$

Plot of $\ln(C_0/C_t)$ vs. time (Fig. 11) yields the k_{app}. The linear relationship between $\ln(C_0/C_t)$ and time (t), is consistent with the first-order kinetics. Finally, Eq. (28) was obtained by assuming $C_t = 0.5C_0$ and Eq. (25) [54].

$$t_{0.5} = \frac{\ln(2)}{K_{ads}k_{L\text{-}H}}+\frac{0.5C_0}{k_{L\text{-}H}} \quad (28)$$

A plot of $t_{0.5}$ vs. $0.5C_0$ yielded the straight line (Fig. 12), whose slope is $1/k_{L\text{-}H}$ and slope/intercept is $0.963/K_{ads}k_{L\text{-}H}$.

For all of the samples, an increase in the dye concentration resulted in a decreased k_{app} (Table 2). The calculated amounts of $k_{L\text{-}H}$ and K_{ads} for various nphs were summarized in Table 3.

3.9. Photo-mineralization of RBO KN-5R

Although, complete dye photo-decolorization often occurred in a short period of time, this does not mean that the photo-mineralization occurred completely. The intermediates formed through the photo-decolorization may be more toxic than the original dye. Therefore, investigating the photo-mineralization efficiency also is necessary.

To evaluate the photo-mineralization of the dye, TOC test was conducted in the optimum condition (pH 6, $[H_2O_2]_0$ = 100 mg/L, [RBO KN-5R] = 40 mg/L, ZnO/TiO_2 = 1:1). As shown in Fig. 13, the photo-decolorization was occurred faster than photo-mineralization. The constant level of TOC in the solution after an extended irradiation time (120 min) suggested that the end products cannot be completely mineralized over this time. Therefore, more time was required for complete photo-mineralization.

The changes in the UV–Vis absorption spectra of RBO KN-5R solutions during UV irradiation at the optimum condition are shown in Fig. 14. RBO KN-5R has a chromophore of –N=N– unit, benzene rings and naphthalene rings (Fig. 2), all of which are stable. The typical spectrum of RBO KN-5R is identified by two bands in the visible region (494 and 386 nm) and two bands in the UV region (297 and 254 nm).

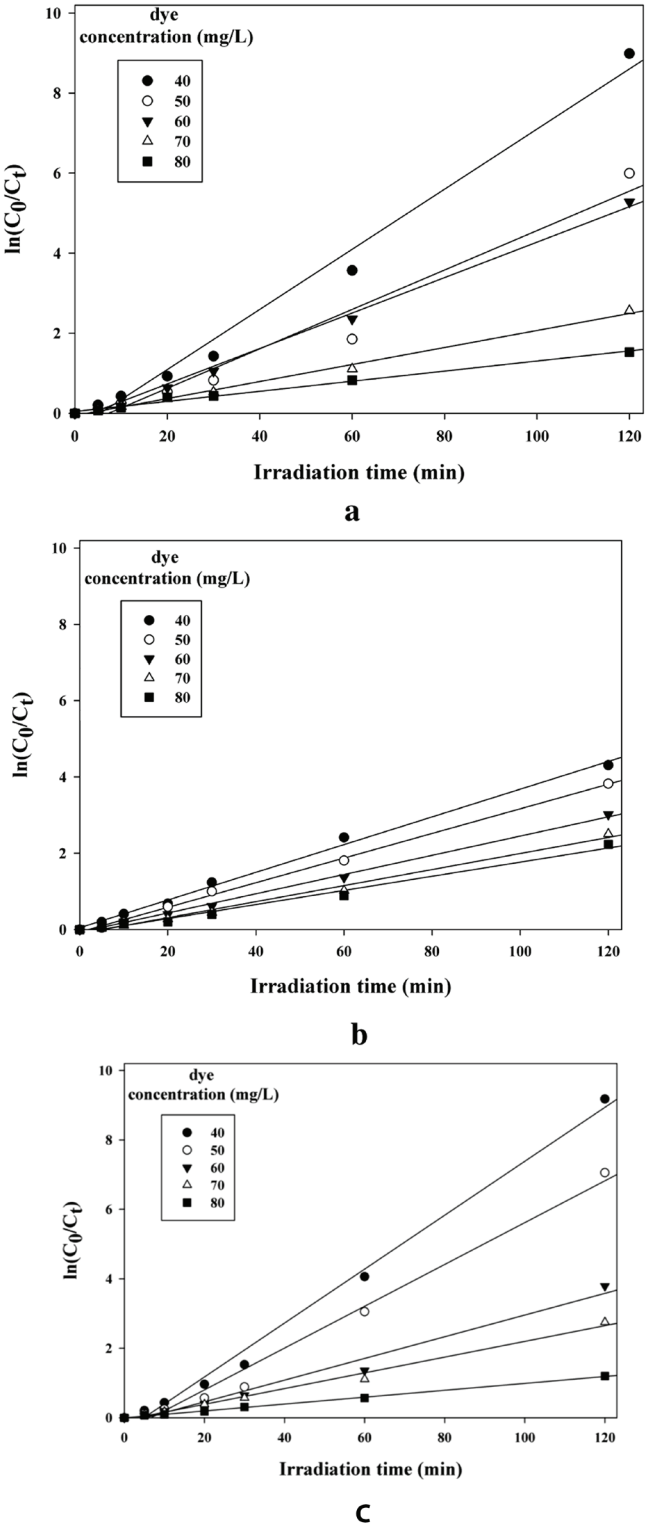

Fig. 11. Plots of $\ln(C_0/C_t)$ vs. irradiation time for different initial concentrations of RBO KN-5R (a) ZnO (b) ZnO\ TiO_2 (c) TiO_2.

The absorbance peaks at 254 and 297 nm are related to $\pi \rightarrow \pi^*$ transitions in the benzene and naphthalene rings of RBO KN-5R, respectively [49]. Photo-degradation of the aromatic part of the dye is confirmed by a reduction in

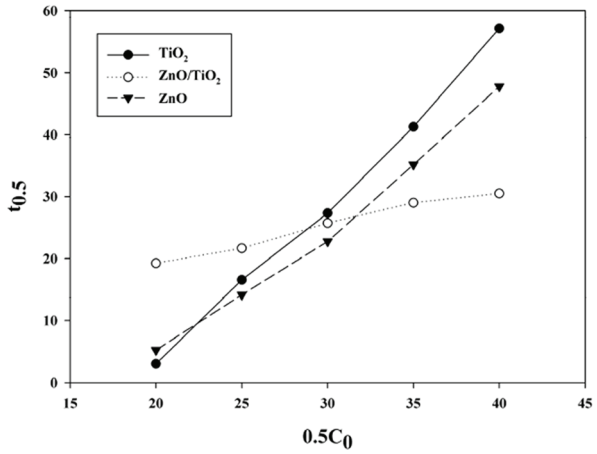

Fig. 12. Plot of $t_{0.5}$ vs. $0.5C_0$ for RBO KN-5R.

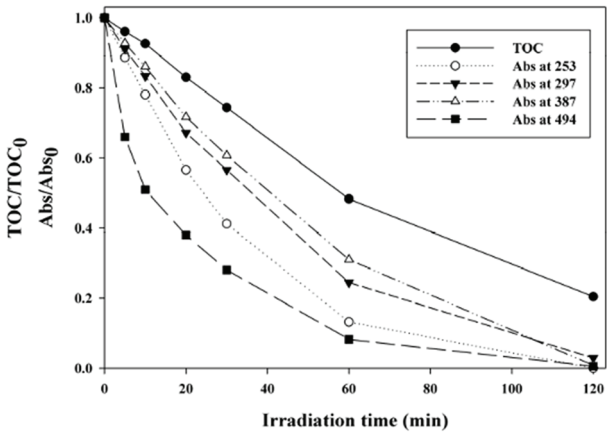

Fig. 13. Decolorization and TOC reduction during the photo-decolorization of RBO KN-5R: pH 6, $[RBO\ KN\text{-}5R]_0$ = 40 mg/L, $[H_2O_2]_0$ = 100 mg/L, ZnO/TiO_2.

Table 2
k_{app} and R^2 for the effect of different initial RBO KN-5R on the photo-decolorization rate

Nphs ratio	Dye concentration (mg/L)					
		40	50	60	70	80
ZnO	k_{app}	0.0596	0.0395	0.0311	0.0185	0.0138
	R^2	0.988	0.995	0.996	0.999	0.976
[ZnO/TiO_2]	k_{app}	0.0679	0.034	0.0227	0.0186	0.0094
	R^2	0.981	0.994	0.997	0.999	0.996
TiO_2	k_{app}	0.0596	0.0395	0.0311	0.0185	0.0138
	R^2	0.988	0.955	0.996	0.999	0.976

the absorbance of UV region. The disappearance of the absorption peaks in the visible region implies that the main chromophore of RBO KN-5R (−N=N−) was destroyed and therefore, the dye solutions became photo-decolorized. It is obvious that the intensity of the peaks in the visible and UV regions decreased and no absorption peaks were observed after 120 min of irradiation. Generally, it can be concluded that the di-azo band are susceptible to attack by $OH^{\bullet}$ produced by AOPs [7].

Table 3
Relating kinetic parameters ($k_{L\text{-}H}$, K_{ads} and R^2) on the photo-degradation of RBO KN-5R

Nphs ratio	$k_{L\text{-}H}$	K_{ads}	R^2
ZnO	0.4815	0.0277	0.995
[ZnO/TiO_2]	0.8161	0.0417	0.885
TiO_2	0.7137	0.0318	0.965

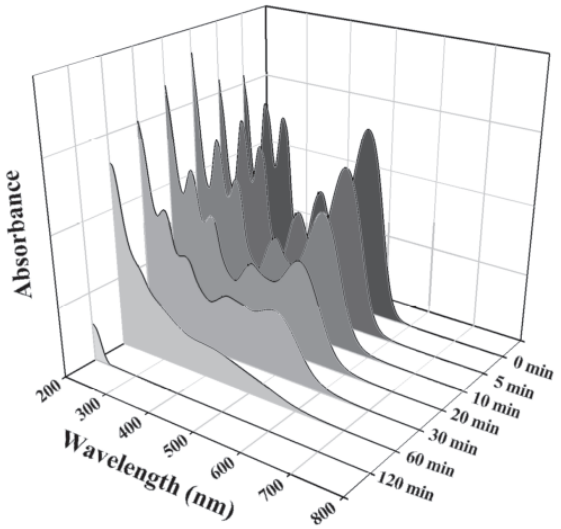

Fig. 14. Changes in the absorption spectrums of RBO KN-5R (40 mg/L): pH 6, $[H_2O_2]_0$ = 100 mg/L, ZnO/TiO_2 at different time intervals of irradiation.

4. Conclusion

Reactive Brilliant Orange KN-5R was successfully photo-decolorized using loaded ZnO, TiO_2 and ZnO/TiO_2 on the spacer fabrics. The effects of operational parameters including pH, initial H_2O_2 concentration, initial dye concentration, nphs composition and various anions were investigated and optimized. SEM images confirmed the loading of nphs on spacers by simple padding process. FTIR spectra confirmed the crosslinking reaction between carboxyl groups of CA, functional groups of the spacer fabric and the nphs. ZnO/TiO_2 NPs, 40 mg/L of initial concentration of the dye, pH 6 and the concentration of 100 mg/L of H_2O_2 were considered as the optimum conditions for the decolorization process. $NaHCO_3$ showed the strongest inhibition effect on the photo-decolorization efficiency followed by NaCl and Na_2SO_4. Almost 90% photo-mineralization of the dye was obtained after 120 min under the optimum condition. The photocatalytic degradation of RBO KN-5R followed the Langmuir–Hinshelwood mechanism. The porous structure of the spacer could provide more time for the photocatalytic reactions through a reduced flowability of the solution. Therefore, the

spacer fabrics treated with the nphs can be regarded as an effective system for photo-decolorization and photo-mineralization of reactive dyes in wastewater.

References

[1] A.A. Telke, D.C. Kalyani, V.V. Dawkar, S.P. Govindwar, Influence of organic and inorganic compounds on oxidoreductive decolorization of sulfonated azo dye CI Reactive Orange 16, J. Hazard. Mater., 172 (2009) 298–309.

[2] H. Wang, C. Xie, W. Zhang, S. Cai, Z. Yang, Y. Gui, Comparison of dye degradation efficiency using ZnO powders with various size scales, J. Hazard. Mater., 141 (2007) 645–652.

[3] S.M. Ghoreishian, K. Badii, M. Norouzi, A. Rashidi, M. Montazer, M. Sadeghi, M. Vafaee, Decolorization and mineralization of an azo reactive dye using loaded nano-photocatalysts on spacer fabric: kinetic study and operational factors, J. Taiwan Inst. Chem. Eng., 45 (2014) 2436–2446.

[4] P.A. Pekakis, N.P. Xekoukoulotakis, D. Mantzavinos, Treatment of textile dyehouse wastewater by TiO2 photocatalysis, Water Res., 40 (2006) 1276–1286.

[5] A.K. Verma, R.R. Dash, P. Bhunia, A review on chemical coagulation/flocculation technologies for removal of colour from textile wastewaters, J. Environ. Manage., 93 (2012) 154–168.

[6] F. Han, V.S.R. Kambala, M. Srinivasan, D. Rajarathnam, R. Naidu, Tailored titanium dioxide photocatalysts for the degradation of organic dyes in wastewater treatment: a review, Appl. Catal., A, 359 (2009) 25–40.

[7] M. Rauf, M. Meetani, S. Hisaindee, An overview on the photocatalytic degradation of azo dyes in the presence of TiO2 doped with selective transition metals, Desalination, 276 (2011) 13–27.

[8] S.M. Ghoreishian, K. Badii, M. Norouzi, K. Malek, Effect of cold plasma pre-treatment on photocatalytic activity of 3D fabric loaded with nano-photocatalysts: response surface methodology, Appl. Surf. Sci., 365 (2016) 252–262.

[9] M. Norouzi, Y. Zare, P. Kiany, Nanoparticles as effective flame retardants for natural and synthetic textile polymers: application, mechanism, and optimization, Polym. Rev., 55 (2015) 531–560.

[10] M. Norouzi, L. Maleknia, Photocatalytic effects of nanoparticles of TiO2 in order to design self-cleaning textiles, Asian J. Chem., 22 (2010) 5930–5936.

[11] A. Akyol, M. Bayramoğlu, Photocatalytic degradation of Remazol Red F3B using ZnO catalyst, J. Hazard. Mater., 124 (2005) 241–246.

[12] A. Aleboyeh, Y. Moussa, H. Aleboyeh, The effect of operational parameters on UV/H2 O2 decolourisation of Acid Blue 74, Dyes Pigm., 66 (2005) 129–134.

[13] M.S.T. Gonçalves, E.M. Pinto, P. Nkeonye, A.M. Oliveira-Campos, Degradation of CI Reactive Orange 4 and its simulated dyebath wastewater by heterogeneous photocatalysis, Dyes Pigm., 64 (2005) 135–139.

[14] Z. Zainal, C.Y. Lee, M.Z. Hussein, A. Kassim, N.A. Yusof, Effect of supporting electrolytes in electrochemically-assisted photodegradation of an azo dye, J. Photochem. Photobiol., A, 172 (2005) 316–321.

[15] S. Chakrabarti, B.K. Dutta, Photocatalytic degradation of model textile dyes in wastewater using ZnO as semiconductor catalyst, J. Hazard. Mater., 112 (2004) 269–278.

[16] N. Barka, S. Qourzal, A. Assabbane, A. Nounah, Y. Ait-Ichou, Factors influencing the photocatalytic degradation of Rhodamine B by TiO2-coated non-woven paper, J. Photochem. Photobiol., A, 195 (2008) 346–351.

[17] M. Hofer, D. Penner, Thermally stable and photocatalytically active titania for ceramic surfaces, J. Eur. Ceram. Soc., 31 (2011) 2887–2896.

[18] C.S. Ryu, M. Kim, B. Kim, Photodegradation of alachlor with the TiO2 film immobilised on the glass tube in aqueous solution, Chemosphere, 53 (2003) 765–771.

[19] M. Nawi, S. Sabar, A. Jawad, W.W. Ngah, Adsorption of reactive red 4 by immobilized chitosan on glass plates: towards the design of immobilized TiO2–chitosan synergistic photocatalyst-adsorption bilayer system, Biochem. Eng. J., 49 (2010) 317–325.

[20] T. Kim, C. Park, J. Yang, S. Kim, Comparison of disperse and reactive dye removals by chemical coagulation and Fenton oxidation, J. Hazard. Mater., 112 (2004) 95–103.

[21] E.R. Trotman, *Dyeing and chemical technology of textile fibres*, Wiley (1984).

[22] M. Norouzi, S.M. Boroujeni, N. Omidvarkordshouli, M. Soleimani, Advances in skin regeneration: application of electrospun scaffolds, Adv. Healthc. Mater., 4 (2015) 1114–1133.

[23] M. Norouzi, I. Shabani, F. Atyabi, M. Soleimani, EGF-loaded nanofibrous scaffold for skin tissue engineering applications, Fiber Polym., 16 (2015) 782–787.

[24] L. Azfarniam, M. Norouzi, Multifunctional polyester fabric using a multicomponent treatment, Fiber Polym., 17 (2016) 298–304.

[25] O. Mirdailami, M. Soleimani, R. Dinarvand, M.R. Khoshayand, M. Norouzi, A. Hajarizadeh, M. Dodel, F. Atyabi, Controlled release of rhEGF and rhbFGF from electrospun scaffolds for skin regeneration, J. Biomed. Mater. Res. A, 103 (2015) 3374–3385.

[26] S.M. Ghoreishian, L. Maleknia, H. Mirzapour, M. Norouzi, Antibacterial properties and color fastness of silk fabric dyed with turmeric extract, Fiber Polym., 14 (2013) 201–207.

[27] A. Nazari, M. Montazer, A. Rashidi, M. Yazdanshenas, M.B. Moghadam, Optimization of cotton crosslinking with polycarboxylic acids and nano TiO2 using central composite design, J. Appl. Polym. Sci., 117 (2010) 2740–2748.

[28] S. Hashemikia, M. Montazer, Sodium hypophosphite and nano TiO2 inorganic catalysts along with citric acid on textile producing multi-functional properties, Appl. Catal., A, 417 (2012) 200–208.

[29] M. Parvinzadeh, S. Moradian, A. Rashidi, M. Yazdanshenas, Effect of the addition of modified nanoclays on the surface properties of the resultant polyethylene terephthalate/clay nanocomposites, Polym. Plast. Technol. Eng., 49 (2010) 874–884.

[30] B. Mistry, *A handbook of spectroscopic data chemistry: UV, IR, PMR, CNMR and mass spectroscopy*, Oxford Book Company, Jaipur, India, 2009.

[31] M.P. Gashti, A. Almasian, M.P. Gashti, Preparation of electromagnetic reflective wool using nano-ZrO 2/citric acid as inorganic/organic hybrid coating, Sens. Actuators A Phys., 187 (2012) 1–9.

[32] M.P. Gashti, F. Alimohammadi, A. Shamei, Preparation of water-repellent cellulose fibers using a polycarboxylic acid/hydrophobic silica nanocomposite coating, Surf. Coat. Tech., 206 (2012) 3208–3215.

[33] M. Barakat, Adsorption and photodegradation of Procion yellow H-EXL dye in textile wastewater over TiO2 suspension, J. Hydro-Environ. Res., 5 (2011) 137–142.

[34] M. Montazer, M. Jolaei, β-Cyclodextrin stabilized on three-dimensional polyester fabric with different crosslinking agents, J. Appl. Polym. Sci., 116 (2010) 210–217.

[35] Y. Jiang, Y. Sun, H. Liu, F. Zhu, H. Yin, Solar photocatalytic decolorization of CI Basic Blue 41 in an aqueous suspension of TiO2–ZnO, Dyes Pigm., 78 (2008) 77–83.

[36] N. Daneshvar, D. Salari, A. Khataee, Photocatalytic degradation of azo dye acid red 14 in water on ZnO as an alternative catalyst to TiO2, J. Photochem. Photobiol., A, 162 (2004) 317–322.

[37] M. Movahedi, A. Mahjoub, S. Janitabar-Darzi, Photodegradation of Congo Red in aqueous solution on ZnO as an alternative catalyst to TiO2, J. Iran. Chem. Soc., 6 (2009) 570–577.

[38] N.M. Mahmoodi, M. Arami, N.Y. Limaee, N.S. Tabrizi, Kinetics of heterogeneous photocatalytic degradation of reactive dyes in an immobilized TiO2 photocatalytic reactor, J. Colloid. Interface Sci., 295 (2006) 159–164.

[39] N.M. Mahmoodi, M. Arami, N.Y. Limaee, Photocatalytic degradation of triazinic ring-containing azo dye (Reactive Red 198) by using immobilized TiO2 photoreactor: bench scale study, J. Hazard. Mater., 133 (2006) 113–118.

[40] H. Coleman, V. Vimonses, G. Leslie, R. Amal, Degradation of 1, 4-dioxane in water using TiO2 based photocatalytic and H2 O2/UV processes, J. Hazard. Mater., 146 (2007) 496–501.

[41] M. Muruganandham, N. Shobana, M. Swaminathan, Optimization of solar photocatalytic degradation conditions of Reactive Yellow 14 azo dye in aqueous TiO2, J. Mol. Catal. A Chem., 246 (2006) 154–161.

[42] H. Katsumata, S. Koike, S. Kaneco, T. Suzuki, K. Ohta, Degradation of Reactive Yellow 86 with photo-Fenton process driven by solar light, J. Environ. Sci., 22 (2010) 1455–1461.
[43] M. Saquib, M. Muneer, Semiconductor mediated photocatalysed degradation of an anthraquinone dye, Remazol Brilliant Blue R under sunlight and artificial light source, Dyes Pigm., 53 (2002) 237–249.
[44] V. Kandavelu, H. Kastien, K.R. Thampi, Photocatalytic degradation of isothiazolin-3-ones in water and emulsion paints containing nanocrystalline TiO2 and ZnO catalysts, Appl. Catal., B, 48 (2004) 101–111.
[45] C. Tang, V. Chen, The photocatalytic degradation of reactive black 5 using TiO2/UV in an annular photoreactor, Water Res., 38 (2004) 2775–2781.
[46] N. Sobana, M. Swaminathan, The effect of operational parameters on the photocatalytic degradation of acid red 18 by ZnO, Sep. Purif. Technol., 56 (2007) 101–107.
[47] M. Muruganandham, N. Sobana, M. Swaminathan, Solar assisted photocatalytic and photochemical degradation of Reactive Black 5, J. Hazard. Mater., 137 (2006) 1371–1376.
[48] S. Kamble, S. Sawant, V. Pangarkar, Photocatalytic mineralization of phenoxyacetic acid using concentrated solar radiation and titanium dioxide in slurry photoreactor, Chem. Eng. Res. Des., 84 (2006) 355–362.
[49] M. Zhang, T. An, X. Hu, C. Wang, G. Sheng, J. Fu, Preparation and photocatalytic properties of a nanometer ZnO–SnO 2 coupled oxide, Appl. Catal., A, 260 (2004) 215–222.
[50] C. Chen, Degradation pathways of ethyl violet by photocatalytic reaction with ZnO dispersions, J. Mol. Catal. A Chem., 264 (2007) 82–92.
[51] D.S. Bhatkhande, S.P. Kamble, S.B. Sawant, V.G. Pangarkar, Photocatalytic and photochemical degradation of nitrobenzene using artificial ultraviolet light, Chem. Eng. J., 102 (2004) 283–290.
[52] I.K. Konstantinou, T.A. Albanis, TiO2-assisted photocatalytic degradation of azo dyes in aqueous solution: kinetic and mechanistic investigations: a review, Appl. Catal., B, 49 (2004) 1–14.
[53] M.N. Chong, B. Jin, Photocatalytic treatment of high concentration carbamazepine in synthetic hospital wastewater, J. Hazard. Mater., 199 (2012) 135–142.
[54] A.N. Rao, B. Sivasankar, V. Sadasivam, Kinetic studies on the photocatalytic degradation of Direct Yellow 12 in the presence of ZnO catalyst, J. Mol. Catal. A Chem., 306 (2009) 77–81.